Curcumin inhibits the activity of ubiquitin ligase Smurf2 to promote NLRP3-dependent pyroptosis in non-small cell lung cancer cells

YUNZHU XI[1,2], SAILI ZENG[1,2], XIAOWU TAN[1,2] and XIAOYU DENG[1,2]

[1]Department of Pulmonary and Critical Care Medicine, The Second Affiliated Hospital, University of South China, Hengyang, Hunan 421000, P.R. China; [2]Hengyang Medical School, University of South China, Hengyang, Hunan 421000, P.R. China

Received September 18, 2024; Accepted January 15, 2025

DOI: 10.3892/ijo.2025.5727

Abstract. Non-small cell lung cancer (NSCLC) is a malignant tumor of significant clinical relevance. Curcumin has been investigated for its potential anticancer properties, as it has been reported to act through multiple cancer-related targets and pathways. The present study aimed to explore the effects of curcumin in NSCLC using both *in vitro* and *in vivo* models. NSCLC cell lines (specifically, A549 and NCI-H1299 cells), and a mouse tumor model established through the subcutaneous injection of A549 cells, were utilized to evaluate the effects of curcumin intervention. The effects of treatment with curcumin on NOD-like receptor pyrin domain-containing 3 (NLRP3) ubiquitination, cell pyroptosis and pyroptosis-associated factors were also evaluated. In addition, Smad ubiquitination regulatory factor 2 (Smurf2) was analyzed via a series of knockdown and overexpression experiments, both *in vitro* and *in vivo*, aimed at investigating its association with curcumin and NLRP3. The results obtained from these experiments showed that curcumin inhibited NSCLC cell growth, promoted pyroptosis and reduced the level of NLRP3 ubiquitination. NLRP3 knockdown reversed the curcumin-induced increase in pyroptosis-associated factors both *in vitro* and *in vivo*. Additionally, Smurf2 interacted with NLRP3 and alterations in Smurf2 expression levels influenced NLRP3 ubiquitination and cell pyroptosis. Moreover, molecular docking analysis demonstrated that curcumin could bind directly to Smurf2, which subsequently led to an inhibition of Smurf2 activity. Knockdown of Smurf2 enhanced curcumin's ability to stabilize NLRP3 and to promote pyroptosis, whereas Smurf2 overexpression negated these effects. In the *in vivo* animal model, curcumin treatment led to reduced tumor volumes and weights, in addition to a decreased expression level of Ki67 and increased expression levels of NLRP3 and pyroptosis-associated factors. Similarly, these effects were enhanced or reversed by Smurf2 knockdown or overexpression, respectively. In conclusion, the findings of the present study showed that curcumin inhibited Smurf2 activity, thereby promoting NLRP3-dependent pyroptosis in NSCLC cells. In addition, these findings have provided mechanistic insights into the role of curcumin in NSCLC, opening an avenue for its potential therapeutic application.

Correspondence to: Dr Xiaoyu Deng, Department of Pulmonary and Critical Care Medicine, The Second Affiliated Hospital, University of South China, 30 Jiefang Road, Hengyang, Hunan 421000, P.R. China
E-mail: 13789355762@163.com

Key words: curcumin, smad ubiquitination regulatory factor 2, NOD-like receptor pyrin domain-containing 3, pyroptosis, non-small cell lung cancer

Introduction

Non-small cell lung cancer (NSCLC) is a prevalent malignancy that represents a significant global health concern (1). There were >1.5 million new cases of lung cancer from 2010 to 2017, of which ~85.3% were NSCLC (2). Patients with NSCLC often face challenges that are associated with the limited treatment options available and poor prognoses, and these severely impact survival outcomes (3). Despite the advancements that have been made in terms of diagnostic and therapeutic strategies, the overall survival rates for NSCLC remain low at ~26.4% (2), due to factors such as drug resistance and adverse treatment effects (4). Therefore, there is an urgent need to identify novel therapeutic interventions for NSCLC and to elucidate their underlying mechanisms of action.

It has been previously shown that dietary polyphenols exert antitumor effects, including their ability to inhibit cancer initiation and progression (5). Among these compounds, curcumin is a natural polyphenolic compound derived from turmeric root that exhibits anti-inflammatory, antioxidant and antitumor pharmacological activities (6). In lung cancer research, curcumin has been shown to possess potential antitumor effects through the modulation of various targets and pathways, such as STAT3, EGFR and PI3K/Akt/mTOR (7). In view of these research findings, we surmised that curcumin may serve as a promising candidate for NSCLC therapy.

Pyroptosis is a form of programmed cell death that is regulated by both intra- and extracellular environmental stimuli (8). This process is characterized by increased membrane permeability, cellular organelle destruction and eventual cell lysis

and collapse (9). Cancer cell pyroptosis has shown promise as a strategy enabling the inhibition of tumor growth and metastasis (9). A previous study reported that natural compounds are able to induce pyroptosis in cancer cells by targeting inflammasomes (10). For example, cucurbitacin B was shown to inhibit NSCLC progression via Toll-like receptor 4/NOD-like receptor pyrin domain-containing 3 (NLRP3)/gasdermin D (GSDMD)-dependent cell pyroptosis (11). Moreover, curcumin was also found to induce pyroptosis in breast cancer cells through NLRP3 inflammasome activation (12). Furthermore, the NLRP3 inflammasome serves an essential role in cancer cell pyroptosis (13). In response to various stress signals, NLRP3 becomes activated and cleavage of the precursor forms of the inflammatory cytokines IL-1β and IL-18 into their biologically active forms occurs (14). On the basis of these findings, it was hypothesized that inducing NLRP3-dependent cell pyroptosis may represent an effective strategy for inhibiting cancer progression, including in cases of NSCLC.

Activation of the NLRP3 inflammasome can be triggered by various stimuli such as pathogenic microorganisms and danger signals, which complicates efforts to target NLRP3 directly (15). Nevertheless, emerging evidence has suggested that modulating NLRP3 ubiquitination and deubiquitination may offer a promising therapeutic strategy for influencing activity of the NLRP3 inflammasome (16,17). A previous study demonstrated that overexpression of Smad ubiquitination regulatory factor 2 (Smurf2) promotes the ubiquitination of Forkhead box O4 and suppresses pyroptosis in oxygen-glucose deprivation/reperfusion-induced cortical neurons (18). Moreover, the upregulation of Smurf2 expression has been observed to be associated with the occurrence, progression and migration of lung cancer (19). However, at present, limited evidence is available on whether Smurf2 is able to regulate NLRP3 ubiquitination and influence pyroptosis in NSCLC cells, highlighting a gap in our current understanding.

The present study aimed to investigate the potential therapeutic mechanisms underlying the effects of curcumin in NSCLC. To meet this aim, experiments utilizing NSCLC cells were performed and animal models were established, to investigate both the effects of curcumin on Smurf2 activity and its association with NLRP3 signaling and cell pyroptosis. In addition, through examining the interplay between NLRP3-dependent pyroptosis and Smurf2 regulation, the present study sought to identify novel therapeutic targets for NSCLC.

Materials and methods

Cell culture and treatment. The human lung epithelial cell line BEAS-2B (iCell-h023; iCell) was cultured in DMEM (cat. no. D5796; MilliporeSigma) supplemented with 10% Gibco® FBS (cat. no. 10099141; Thermo Fisher Scientific, Inc.) and 1% penicillin/streptomycin (P/S) (cat. no. SV30010; Beyotime Institute of Biotechnology). The NSCLC cell lines A549 (cat. no. CL-0016) and NCI-H1299 (cat. no. CL-0165; both purchased from Procell Life Science & Technology Co., Ltd.) were grown in F-12K medium (cat. no. iCell-0007; iCell) and RPMI-1640 medium (cat. no. R8758; MilliporeSigma) respectively, both supplemented with 10% FBS and 1% P/S. All cells were maintained at 37˚C in a humidified atmosphere containing 5% CO_2.

Pyroptosis assay. Pyroptosis was detected using flow cytometric analysis. To evaluate the role of curcumin in NSCLC cell pyroptosis, the cells were treated with various concentrations of curcumin (0, 2.5, 5, 10, 20 and 40 μM) for 24 h at 37˚C to determine the optimal concentration (20). Curcumin was dissolved in 0.5% DMSO (21) and DMSO concentrations <1% were investigated to confirm a lack of any significant cytotoxicity (22). Subsequently, the NSCLC cells were categorized into the following groups: i) The control (untreated) group; ii) the curcumin (20 μM curcumin; cat. no. 78246; MilliporeSigma) group; iii) the curcumin + VX-765 [20 μM curcumin with 20 μM VX-765 (23)] group; iv) the curcumin + INF39 [20 μM curcumin with 10 μM INF39 (24)] group; and v) the curcumin + disulfram (DSF) [20 μM curcumin with 30 μM DSF (25)] group. VX-765 (cat. no. HY-13205), INF39 (cat. no. HY-101868) and DSF (cat. no. HY-B0240; all purchased from MedChemExpress) were used as inhibitors of caspase-1, NLRP3 and GSDMD, respectively. Cells were treated with curcumin alone or in combination with VX-765/INF39/DSF for 24 h at 37˚C.

Effect of curcumin on NLRP3 expression. To investigate the effect of curcumin (20 μM) on NLRP3, NSCLC cells were divided into four groups, namely, the control, curcumin, MG132 (cat. no. HY-13259; MedChemExpress) and MG132 + curcumin groups. NLRP3 protein expression levels were detected by western blotting. Previous studies have reported that MG132 is a proteasome inhibitor (26, 27). Cells in the MG132 group were treated with 10 μM MG132 for 6 h at 37˚C, whereas those in the MG132 + curcumin group were treated with 10 μM MG132 for 6 h at 37˚C, followed by the application of 20 μM curcumin. To further explore the association between NLRP3 and curcumin, NLRP3 expression was knocked down using short interfering RNAs (siRNAs; si). NSCLC cells were divided into four additional groups, namely, the control, curcumin, curcumin+si-negative control (NC) and curcumin+si-NLRP3 groups. The siRNA sequences used were as follows: the sense si-NC, 5'-TTCTCCGAACGT GTCACGT-3' and antisense si-NC, 5'-ACGTGACACGTT CGGAGAA-3'; and the sense si-NLPR3, 5'-CCGTAAGAA GTACAGAAAGTA-3' and the antisense si-NLPR3, 5'-TAC TTTCTGTACTTCTTACGG-3'. These siRNAs were provided by Honorgene. Cells in the si-NC and si-NLRP3 groups were first transfected with non-targeting siRNA (si-NC) or NLRP3-specific siRNA (si-NLRP3) respectively, prior to subsequent treatment with 20 μM curcumin for 24 h at 37˚C.

Effect of Smurf2 on NLRP3 and pyroptosis. NLRP3 protein expression levels and pyroptosis were detected by western blotting and flow cytometric analysis, respectively. NSCLC cells were divided into four groups, namely, the control, overexpression (oe)-NC, oe-Smurf2 and oe-Smurf2 + MG132 groups. Cells in the oe-NC and oe-Smurf2 groups were transfected with either an empty vector (oe-NC) or a Smurf2 overexpression plasmid (oe-Smurf2), respectively. The plasmid backbone of oe-Smurf2 was pUC19 (cat. no. N3041L; New England BioLabs, Inc.). For the oe-Smurf2 + MG132 group, cells were

first transfected with oe-Smurf2 and subsequently treated with 10 μM MG132 for 6 h at 37˚C. Additionally, to further explore the relationship between Smurf2 and NLRP3, cells were categorized into five groups, namely, the control, si-NC, si-Smurf2, si-Smurf2 + si-NC and si-Smurf2 + si-NLRP3 groups. The sense sequence of si-Smurf2 was 5'-GCTGGATTTCTCGGT TGTGTT-3' and the antisense si-Smurf2 sequence was 5'-ACA ACACCGAGAAATCCAGC-3'. These siRNAs were provided by Honorgene. Cells in the si-NC and si-Smurf2 groups were transfected with si-NC or si-Smurf2, respectively, whereas for the si-Smurf2 + si-NC and si-Smurf2 + si-NLRP3 groups, cells were co-transfected with si-Smurf2 together with either si-NC or si-NLRP3.

Association between Smurf2 and curcumin. To investigate the association between Smurf2 and curcumin (20 μM), NSCLC cells were separated into six groups; namely, the control, curcumin, curcumin + si-NC, curcumin + si-Smurf2, curcumin + oe-NC and curcumin + oe-Smurf2 groups. The results of this experiment were determined by western blotting and flow cytometric analysis. Cells in the si-NC and si-Smurf2 groups were transfected with si-NC or si-Smurf2, respectively, whereas cells in the oe-NC and oe-Smurf2 groups were transfected with either empty vector or the Smurf2 overexpression plasmid. All groups were treated with 20 μM curcumin following transfection for 24 h at 37˚C.

Cell transfection. Cells were transfected with the plasmids using Lipofectamine™ 2000 transfection reagent (cat. no. 11668019; Thermo Fisher Scientific, Inc.). Samples were prepared with 95 μl of serum-free medium per tube, then 5 μl of siRNA (3 μg) and 5 μl of Lipofectamine™ 2000 were added to the samples, respectively. After incubating at 22˚C for 5 min, the samples were mixed and incubated at 22˚C for 20 min. Finally, the mixture was homogenized into the transfected wells and incubated at 37˚C for 6 h. Subsequent experiments were performed after 48 h of transfection.

Animal experiments. Male nude mice (weight, 14-15 g; aged, 4 weeks) were obtained from Hunan SJA Laboratory Animal Co., Ltd. The mice were kept in an environment of 25±2˚C, 50±5% humidity and a 12-hour light-dark cycle with free access to food and water. After a 7 day acclimatization period, NSCLC *in vivo* models were established as described previously (28). Briefly, $2x10^6$ A549 cells (100 μl) were resuspended in PBS (cat. no. AWC0409; Changsha Abiwei Biotechnology Co., Ltd.) and injected subcutaneously into the dorsal side of each mouse. The total number of mice used was 30. The tumor volume was recorded every 3 days using the formula: Volume=0.5 x length x width^2. The maximum tumor volume we observed was 999.35 mm^3. At 7 days following injection, the formation of tumors was confirmed and intervention procedures were subsequently initiated.

To investigate the association between curcumin and NLRP3 *in vivo*, the mice were divided into four groups (n=3/group), namely, the model, model + curcumin, model$^{si\text{-}NC}$ + curcumin and model$^{si\text{-}NLRP3}$ + curcumin groups. The model group comprised untreated NSCLC nude mice, whereas the model + curcumin group received curcumin treatment via intraperitoneal injection (30 mg/kg) once daily for 14 consecutive days (29). The model$^{si\text{-}NC}$ + curcumin and model$^{si\text{-}NLRP3}$ + curcumin groups were established by injecting $2x10^6$ A549 cells (100 μl) transfected with si-NC or si-NLRP3 into the mice, followed by the same curcumin treatment regimen.

Furthermore, to evaluate the correlation between curcumin and Smurf2 *in vivo*, the mice were separated into six groups (n=3/group), namely, the model, model+curcumin, model$^{si\text{-}NC}$ + curcumin, model$^{si\text{-}Smurf2}$ + curcumin, model$^{oe\text{-}NC}$ + curcumin and model$^{oe\text{-}Smurf2}$ + curcumin groups. In these groups, the nude mice were injected with A549 cells ($2x10^6$ cells in 100 μl) transfected with si-NC or si-Smurf2 or oe-NC or oe-Smurf2 to initiate tumorigenesis, followed by subsequent curcumin intervention.

At the end of the experiments, the mice were euthanized by intravenous injection with 150 mg/kg sodium pentobarbital (30) (cat. no. P3761; Merck KGaA). Mice were determined to be dead when their breathing and heartbeat stopped and their pupils dilated. The humane endpoint we used was a tumor volume that reached 10% of the mouse's body weight (approximately 2,000 mm^3). There were no animals that reached the humane endpoint before the end of the experiment. Tumors and peripheral blood samples from the tail vein (~0.5 ml) were collected for subsequent analyses. All experimental procedures were approved by the Medical Ethics Committee of the Second Affiliated Hospital, University of South China (approval no. NHFE2022010601).

Cell counting kit-8 (CCK-8) assay. For the CCK-8 assay, cells were digested by trypsin-based digestive solution (cat. no. AWC0232; Changsha Abiwei Biotechnology Co., Ltd.) and seeded at a density of $5x10^3$ cells/well, with three replicate wells set up for each group. Each well was supplemented with 100 μl medium containing 10% CCK-8 solution (cat. no. NU679; Dojindo Laboratories, Inc.). The cells were incubated at 37˚C in an atmosphere containing 5% CO_2 atmosphere for 4 h. Following incubation, the optical density at 450 nm was measured using a microplate reader (cat. no. MB-530; Shenzhen Hele Technology Co., Ltd.).

5-Ethynyl-2'-deoxyuridine (EdU) assay. Cell proliferation was assessed using an EdU assay kit (cat. no. C10310; Guangzhou RiboBio Co., Ltd.). EdU solution was diluted 1:1,000 in cell culture medium and the cells ($5x10^3$ cells/well) were subsequently incubated with 100 μl medium containing 50 μM EdU overnight at 22˚C. Cells were then fixed at 22˚C for 30 min using the fixative provided in the kit and stained sequentially with 1X Apollo staining reaction solution and 1X Hoechst 33342 reaction solution for 1.5 h at room temperature, protected from the light. Subsequently, images were captured using a fluorescence microscope (cat. no. BA210T; Motic Microscopes) and the proliferation rate was calculated as the ratio of EdU-positive cells to Hoechst-stained cells (proliferation rate=EdU:Hoechst) using the ImageJ software (version 1.8.0.112; National Institutes of Health).

Transwell assay. For the migration assay, 500 μl Complete™ medium (cat. no. AW-MC028; Changsha Abiwei Biotechnology Co., Ltd.) containing 10% FBS was added to the lower chamber of a Transwell plate (cat. no. 3428; Corning, Inc.). NSCLC cells undergoing drug treatment were resuspended at

a concentration of $2x10^6$ cells/ml and 100 μl cell suspension was placed in the upper chamber, without serum. Following incubation at 37˚C for 48 h, cells in the upper chamber were removed and the cells on the underside of the membrane that had migrated were transferred to clean wells. The cells were stained with 0.1% crystal violet (cat. no. AWC0333; Shanghai Biotechwell Co., Ltd.) at 22˚C for 5 min, washed with water, visualized using a fluorescence microscope (cat. no. BA210T; Motic Microscopes) and analyzed using ImageJ software (version 1.8.0.112; National Institutes of Health).

For the invasion assay, the EP tubes, Matrigel™ (cat. no. 354262; Becton, Dickinson and Company) and Transwell inserts were preconditioned at 4˚C overnight. On the day of the experiment, Matrigel was diluted to a final concentration of 200 μg/well and added to the upper chamber. Following incubation at 37˚C for 30 min, the supernatant was aspirated and the remaining steps were performed as described for the migration assay above. The invasive cells were stained with crystal violet at 22˚C for 5 min, visualized using a fluorescence microscope and analyzed using ImageJ software (version 1.8.0.112; National Institutes of Health).

Flow cytometric analysis

Cell cycle assay. NSCLC cells ($2x10^6$ cells/ml) were resuspended in pre-cooled PBS and fixed by adding pre-cooled 100% ethanol dropwise to a final concentration of 75%. The samples were stored at 4˚C overnight. The following day, ethanol was removed by centrifugation at 400 x g for 5 min at 4˚C and the cells were resuspended in pre-cooled PBS. Cells were subsequently stained with PI (cat. no. MB2920; Dalian Meilune Biology Technology Co., Ltd.) working solution at 4˚C for 30 min in the dark. The cell cycle distribution was analyzed using a flow cytometer (cat. no. A00-1-1102; Beckman Coulter, Inc.) and the percentage of cells in each phase was determined from the PI fluorescence histogram. GraphPad Prism 8 (version 8.0.2.263; Dotmatics) was used to produce the PI fluorescence histogram.

Detection of cell pyroptosis. NSCLC cells ($2x10^6$ cells/ml) were collected using trypsin-based digestive solution (cat. no. AWC0232; Changsha Abiwei Biotechnology Co., Ltd.) for 5 min at 22˚C and washed thoroughly. The cells were subsequently treated with caspase-1 working solution (cat. no. ab219935; Abcam) for 5 min at 22˚C, followed by staining with PI for 30 min at 22˚C. The mixture was subsequently incubated at 22˚C for 1 h, protected from the light. Finally, pyroptosis was analyzed using a flow cytometer (cat. no. A00-1-1102; Beckman Coulter, Inc.) and the GraphPad Prism 8 software (version 8.0.2.263; Dotmatics).

Scanning electron microscopy (SEM) analysis. NSCLC cells ($2x10^6$ cells/ml) were fixed with 2.5% glutaraldehyde (cat. no. AWI0097; Changsha Abiwei Biotechnology Co., Ltd.) for 12 h at 22˚C and washed using PBS. Subsequently, cells were treated with 1% osmium acid (cat. no. AWI0136; Changsha Abiwei Biotechnology Co., Ltd.) for 2 h at 22˚C. Dehydration was performed sequentially using increasing concentrations of ethanol (30, 50, 70, 80, 90, 95 and 100%; 15 min/concentration), after which the samples were treated with a 1:1 mixture of 100% ethanol and isoamyl acetate (cat. no. 10003118; Sinopharm Chemical Reagent Co., Ltd.) for 30 min at 22˚C. After overnight drying at 22˚C, the samples were observed using an SEM microscope (Helios 5 UC; Thermo Fisher Scientific, Inc.) and analyzed using ImageJ software (version 1.8.0.112; National Institutes of Health).

Western blot analysis. Total protein was extracted from cells ($2x10^6$ cells/ml) and the tumor tissues of nude mice using 300 μl RIPA lysis buffer (cat. no. R0010; Beijing Solarbio Science & Technology Co., Ltd.) supplemented with a protease inhibitor cocktail (cat. no. AWH0645) and a protein phosphatase inhibitor (cat. no. AWH0650; both purchased from Changsha Abiwei Biotechnology Co., Ltd.). The BCA protein quantification kit (cat. no. AWB0156, Changsha Abiwei Biotechnology Co., Ltd) was utilized to determine the protein concentration. The densitometry was performed using GraphPad Prism 8 software (version 8.0.2.263; Dotmatics). Protein samples (20 μg) were used for electrophoresis. The constant voltage of electrophoresis was 75 V for 130 min. Subsequently, the proteins were separated using SDS-PAGE (12% gel) and transferred to PVDF membranes pre-treated with methanol (99.8%) for 15 sec at 22˚C. The membranes were blocked with 5% skimmed milk for 90 min at 22˚C and incubated with primary antibodies (Table I) at 4˚C overnight. β-actin was used as the internal reference control. Subsequently, the membranes were incubated with secondary antibodies (Table I) at 37˚C for 1.5 h. Protein bands were visualized using ECL Plus super-sensitive luminescent liquid (cat. no. K-12049-D50; Advansta, Inc.) and imaged using a chemiluminescence imaging system (ChemiScope6100; Clinx Science Instruments Co., Ltd.).

To assess the protein stability of NLRP3, cells were treated with the protein synthesis inhibitor cycloheximide (CHX) at a concentration of 100 μg/ml (cat. no. 583794; Gentihold) for 0, 4, 8 or 12 h at 4˚C (31). Following CHX treatment, proteins were analyzed using the standard western blotting procedure described above.

Co-immunoprecipitation (Co-IP) assay. The cells were washed and lysed using 400 μl of IP cell lysate (cat. no. AWB0144; Changsha Abiwei Biotechnology Co., Ltd.). The lysate was subsequently centrifuged at 4,000 x g for 15 min at 4˚C to isolate the proteins, which were then incubated at 4˚C overnight with NLRP3 antibodies (cat. no. ab263899; Abcam) which was diluted by PBST containing 0.05% Tween 20 (cat. no. AWI0130, Changsha Abiwei Biotechnology Co., Ltd). Subsequently, Protein A/G agarose beads (20 μl) were added to capture the antigen-antibody complexes and the mixture was incubated at 4˚C for 2 h with gentle shaking. The agarose beads were washed four times with 400 μl of IP lysate and the final precipitate was collected. Following Co-IP assay, both the ubiquitination level of NLRP3 and the expression levels of NLRP3 and Smurf2 were analyzed using western blotting analysis, as described above.

ELISA. The concentrations of IL-1β in the cell supernatants and animal serum samples were measured using either a human IL-1β ELISA kit (cat. no. CSB-E08053h) or a mouse IL-1β ELISA kit (cat. no. CSB-E08054m; both kits purchased from Cusabio Technology, LLC), following the manufacturer's instructions. Similarly, the levels of IL-18 were determined using a human IL-18 ELISA kit (cat. no. CSB-E07450h) or

Table I. Antibodies used in the present study.

Antibody target	Cat. no.	Dilution	Supplier
NOD-like receptor pyrin domain-containing 3	ab263899	1:1,000	Abcam
Caspase-1	ab207802	1:1,000	Abcam
Gasdermin D (GSDMD)/cleaved GSDMD	ab225867	1:1,000	Abcam
Smad ubiquitination regulatory factor 2	AWA55626	1:1,000	Changsha Abiwei Biotechnology Co., Ltd.
β-actin	66009-1-Ig	1:5,000	Proteintech Group, Inc.
HRP goat anti-mouse IgG	SA00001-1	1:5,000	Proteintech Group, Inc.
HRP goat anti-rabbit IgG	SA00001-2	1:6,000	Proteintech Group, Inc.

Table II. Primer sequences used in the present study.

Gene	Sequence (5'-3')	Product length, bp
H-NOD-like receptor pyrin domain-containing 3	F: GCCACGCTAATGATCGACT R: TCTTCCTGGCATATCACAGT	170
H- Smad ubiquitination regulatory factor 2	F: CATGTCTAACCCCGGAGGC R: TGCCCAGATCCATCAACCAC	138
H-β-actin	F: ACCCTGAAGTACCCCATCGAG R: AGCACAGCCTGGATAGCAAC	224

F, forward; R, reverse; H, human.

mouse IL-18 ELISA kit (cat. no. CSB-E04609m; both kits purchased from Cusabio Technology, LLC).

Reverse transcription-quantitative PCR (RT-qPCR) assay. Total RNA was extracted from NSCLC cell lines (2x10^6 cells/ml) using TRIzol® reagent (cat. no. 15596026; Invitrogen; Thermo Fisher Scientific, Inc.), following the manufacturer's instructions. RNA was subsequently reverse transcribed into cDNA using an mRNA reverse transcription kit (cat. no. CW2569; Cwbio). The relative expression levels of NLRP3 and Smurf2 were determined using the UltraSYBR Mixture (cat. no. CW2601; Cwbio) on an ABI 7900 system (cat. no. QuantStudio1; Thermo Fisher Scientific, Inc.). The thermocycling conditions used were as follows: Denaturation at 95˚C for 10 min, followed by 40 cycles of 95˚C for 15 sec and 60˚C for 30 sec. The $2^{-\Delta\Delta Cq}$ method was employed to calculate the relative mRNA levels of target genes (32). β-actin used as the internal reference control and the specific primer sequences are shown in Table II.

Hematoxylin and eosin (H&E) staining. Tumor tissues from nude mice were treated with xylene (cat. no. 10023418; Sinopharm Chemical Reagent Co., Ltd.) for 20 min at 22˚C, fol lowed by sequential immersion in a series of decreasing ethanol solutions (100, 100, 95, 85 and 75%; 5 min each). After rinsing the tissues in distilled water for 5 min, tissue sections were stained with hematoxylin (cat. no. AWI0009a; Changsha Abiwei Biotechnology Co., Ltd.) for 10 min at 22˚C, and subsequently with eosin (cat. no. G1100; Beijing Solarbio Science & Technology Co., Ltd.) for 5 min at 22˚C. The sections were dehydrated using gradient ethanol (95-100%), treated with xylene for 10 min at 22˚C, mounted with neutral gum (cat. no. ZLI-9555; Beijing Zhongshan Jinqiao Biotechnology Co., Ltd.) and imaged using an optical microscope (cat. no. BA310E; Motic Microscopes).

Molecular docking analysis. Molecular docking analysis of curcumin with the Smurf2 protein was performed using VINA software (version 1.1.2; Scripps Research). PyMOL software (version 2.3; Schrödinger) was used to visualize binding of the ligand to the receptor-binding pocket and to predict receptor-ligand interactions and binding energies.

Immunohistochemical analysis. Tumor tissues from nude mice were fixed in 4% paraformaldehyde for 30 min at 22˚C. Paraffin sections were 4-5 µm thick. The tissues were treated sequentially with xylene and ethanol of decreasing concentrations (100, 95, 85 and 75%). The tissues were subsequently immersed in 0.01 mol/l citrate buffer (cat. no. ZLI-9065; Beijing Zhongshan Jinqiao Biotechnology Co., Ltd.) and microwaved until the solution began to boil. After cooling to room temperature, the sections were treated with 1% periodic acid (cat. no. BSBA-4245; Beijing Zhongshan Jinqiao Biotechnology Co., Ltd.) to inactivate endogenous enzymes for 15 min at room temperature. The sections were blocked with 3% BSA (cat. no. AWT0368a, Changsha Abiwei Biotechnology Co., Ltd) at 22˚C for 30 min. The primary antibodies against Ki67 (cat. no. 28074-1-AP; 1:400; Proteintech Group, Inc.) were applied and incubated at 4˚C overnight. Subsequently, the sections were incubated with HRP-conjugated goat

anti-rabbit IgG secondary antibodies (1:1,000; Table I) at 37˚C for 30 min, after which the sections were treated with a DAB working solution (cat. no. ZLI-9017; Beijing Zhongshan Jinqiao Biotechnology Co., Ltd.) and counterstained with hematoxylin at 22˚C for 5 min. The tissues were subsequently dehydrated with ethanol in ascending concentrations (60-100%), treated with xylene at 22˚C for 10 min, mounted for fluorescence microscopic (cat. no. BA210T; Motic Microscopes) examination and analyzed using the ImageJ software (version 1.8.0.112; National Institutes of Health).

Bioinformatics analysis. To predict which ubiquitin ligases are associated with NLRP3, bioinformatics analysis was performed using the UbiBrowser 1.0 database (http://ubibrowser.bio-it.cn/ubibrowser/). The data were downloaded from the public repository on the UbiBrowser 1.0 database (http://ubibrowser.bio-it.cn/ubibrowser/strict/networkview/networkview/name/Q96P20/jobId/ubibrowse-I2025-02-06-15867-1738804849). The significance cut-off level used was $P<0.05$.

Statistical analysis. Statistical analysis was performed using GraphPad Prism 8 software (version 8.0.2.263; Dotmatics). All experiments were performed in triplicate and data are expressed as the mean±SD. For data following a normal distribution, comparisons between two groups were performed using the unpaired t-test, whereas comparisons among multiple groups were performed using a one-way ANOVA followed by Tukey's post hoc test. $P<0.05$ was considered to indicate a statistically significant difference.

Results

Curcumin inhibits the growth of NSCLC cells by inducing pyroptosis. To evaluate the role of curcumin in the pyroptosis of NSCLC cells, the IC_{50} of curcumin, reflecting its effect on cell growth, was determined (33). The results showed that the IC_{50} for curcumin in the experiments performed using BEAS-2B cells was 233.6 μM, whereas the IC_{50} values for A549 and NCI-H1299 cells were 14.85 and 13.14 μM, respectively. To effectively inhibit the target activity in the specific cell lines under investigation, the concentration of 20 μM for curcumin was selected for subsequent experiments (Fig. 1A).

To further investigate the association between curcumin and pyroptosis, NSCLC cells were treated either with curcumin alone or in combination with inhibitors of caspase-1 (VX-765), NLRP3 (INF39) or GSDMD (DSF). These results demonstrated that treatment with curcumin led to a significant reduction in the viability (Fig. 1B), proliferation (Fig. 1C), migration (Fig. 1D) and invasion (Fig. 1E) of NSCLC cells compared with untreated controls. However, inhibition of caspase-1, NLRP3 or GSDMD reversed the effects of curcumin on the viability (Fig. 1B), proliferation (Fig. 1C), migration (Fig. 1D) and invasion (Fig. 1E) of cells. Additionally, curcumin intervention resulted in cell cycle arrest in NSCLC cells, which was also reversed by treating the cells with the inhibitors of caspase-1, NLRP3 and GSDMD (Fig. 1F).

Furthermore, treatment with curcumin increased the levels of cell pyroptosis and cell death via pyroptosis when compared with the control group (Fig. 1G). The morphological changes characteristic of pyroptosis, including increased cell swelling, reduced cytoplasmic density and pore formation in the cell membrane, were observed in the curcumin-treated NSCLC cells (Fig. 1H). These changes induced by curcumin, however, were markedly attenuated when caspase-1, NLRP3 or GSDMD inhibitors were added (Fig. 1G and H). Furthermore, the levels of the pyroptosis-associated cytokines, IL-1β and IL-18, in the cell supernatant were increased upon treatment with curcumin (Fig. 1I). Similarly, curcumin treatment increased the expression levels of pyroptosis-associated proteins, including NLRP3, caspase-1, GSDMD and GSDMD-N, but reduced these expression levels upon inhibition of caspase-1, NLRP3 or GSDMD (Fig. 1J). Taken together, these findings suggested that curcumin suppresses the growth of NSCLC cells, potentially through the induction of pyroptosis.

Curcumin induces pyroptosis in NSCLC cell lines and cancerous tissues from NSCLC nude mice via upregulation of NLRP3. Given the close association between NLRP3 and cell pyroptosis (34), the present study aimed to further investigate the association between curcumin and NLRP3. The stability and ubiquitination levels of NLRP3 were assessed in NSCLC cells. The results obtained demonstrated that curcumin increased the protein stability of NLRP3, while reducing its ubiquitination levels (Fig. 2A and B). Moreover, curcumin increased NLRP3 protein expression levels and inhibited its degradation, similar to the effects exhibited by MG132, a proteasome inhibitor (Fig. 2C). The combination of curcumin and MG132 resulted in a higher level of NLRP3 expression compared with curcumin alone, demonstrating that curcumin promotes NLRP3 expression through reducing its ubiquitination, and that this effect is dependent on the proteasomal degradation pathway.

To further elucidate the role of NLRP3 in curcumin's action on NSCLC cells, NLRP3 was knocked down in NSCLC cells. Among the siRNA groups, si-NLRP3#2 exhibited the highest knockdown efficiency and this was therefore used in subsequent experiments (Fig. 2D). Compared with the curcumin + si-NC group, the curcumin + si-NLRP3 group demonstrated a significant decrease in pyroptosis (Fig. 2E) and was associated with significant reductions in the protein expression levels of NLRP3, caspase-1, GSDMD and GSDMD-N in cells (Fig. 2F), as well as marked reductions in the concentrations of IL-1β and IL-18 in the culture supernatant (Fig. 2G). Comparing the results obtained in A549 and NCI-H1299 cells, there was an almost one-fold difference in the level of change of GSDMD expression, which was potentially due to the fact that gene or protein expression levels vary by differing degrees in different types of cells. This finding may also have been due to the cells' unique properties, or the regulatory expression mechanisms, such as cell specificity or cell cycle regulation. Moreover, this approximately one-fold difference in the GSDMD expression level comparing between the curcumin + siNC and curcumin + siNLRP3 groups may have resulted from the effect that knocking down NLRP3 has on reducing the expression levels of GSDMD and GSDMD-N (Fig. 2F). Collectively, these findings suggested that NLRP3 knockdown diminishes the ability of curcumin to induce pyroptosis in NSCLC cells (Fig. 2E-G).

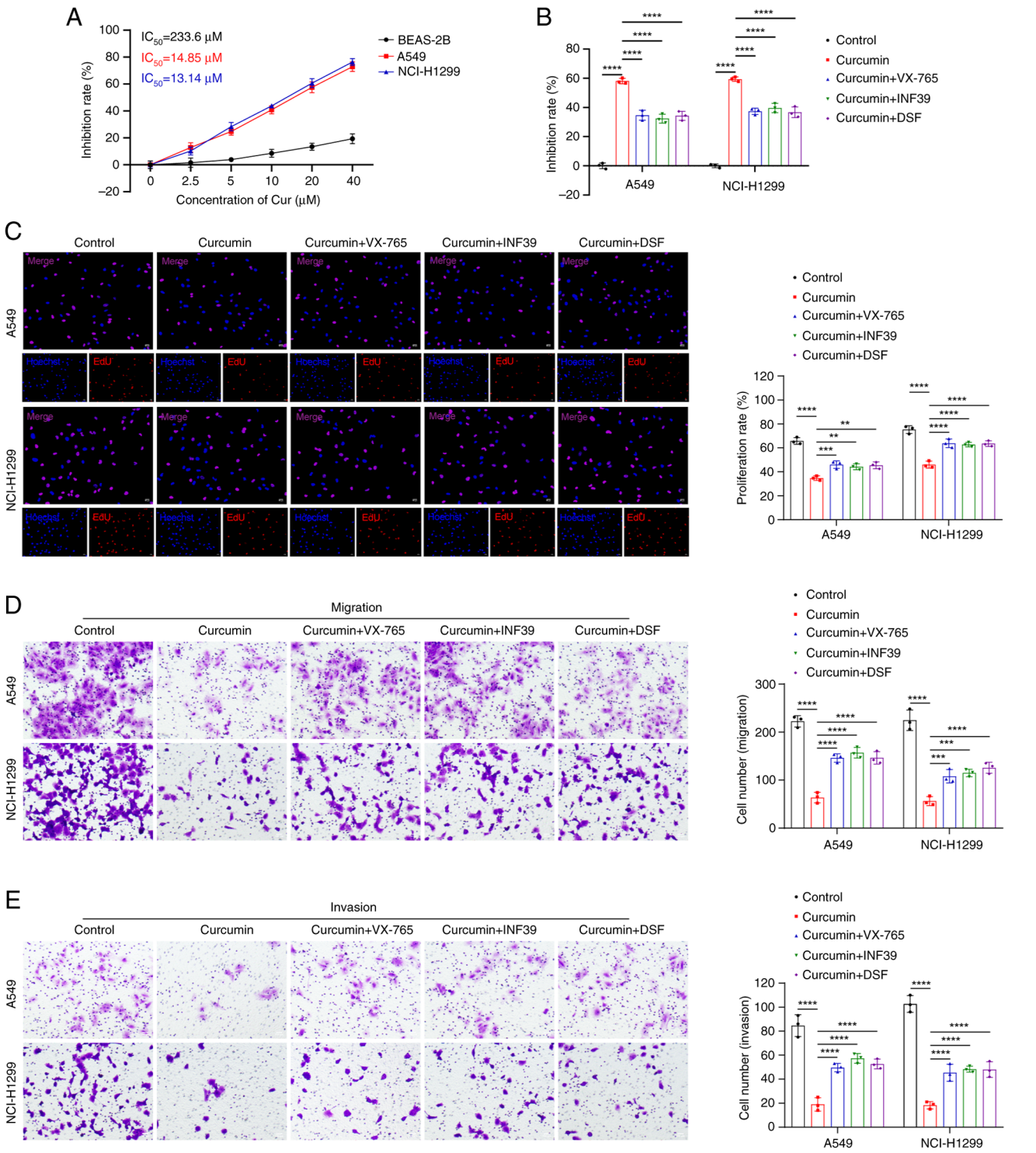

Figure 1. Continued.

To corroborate these findings *in vivo*, experiments were performed using NSCLC nude mouse models (Fig. 2H). These experiments showed that treatment with curcumin led to a significant reduction in tumor volume (Fig. 2I) and weight (Fig. 2K) compared with the model group. Moreover, compared with the model$^{si\text{-}NC}$+curcumin group, the knockdown of NLRP3 caused a significant increase in tumor volume (Fig. 2I) and weight (Fig. 2K), demonstrating that NLRP3 exerted a crucial role in mediating the effects of curcumin. Subsequently, H&E staining further demonstrated that NLRP3 knockdown inhibited curcumin-induced NSCLC cell death in tumor tissues (Fig. 2J). Consistent with the *in vitro* findings, curcumin intervention in tumors led to a significantly increase in the protein expression levels of NLRP3, caspase-1, GSDMD and GSDMD-N, as well significant increases in the concentrations of IL-1β and IL-18 in the serum when compared with the model group. Knockdown of NLRP3 reversed these effects, suppressing curcumin-induced pyroptosis in the NSCLC tumors (Fig. 2L and M). Taken together, the results from both the *in vitro* and the *in vivo* experiments suggested that

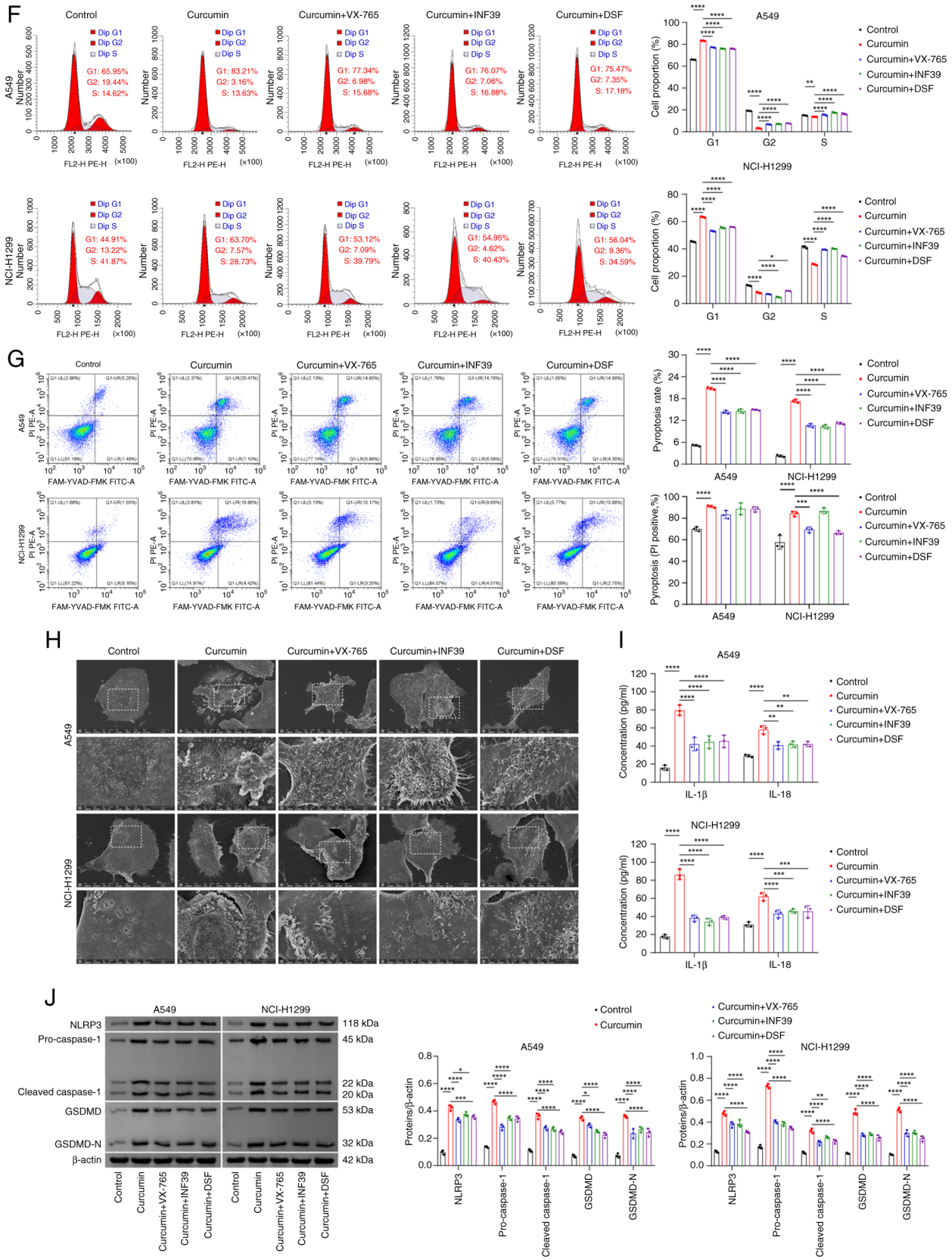

Figure 1. Curcumin inhibits the growth of NSCLC cells by inducing pyroptosis. (A) The IC_{50} value of curcumin was determined by CCK-8 assay. (B) Cell viability of NSCLC cells was assessed using the CCK-8 assay. (C) NSCLC cell proliferation was analyzed via EdU assay. Scale bar, 50 μm. Cell migration (D) and invasion (E) were evaluated by Transwell assays. Scale bar, 100 μm. (F) Cell cycle distribution was analyzed by flow cytometric analysis. (G) Pyroptosis detection was performed via flow cytometry, where UR/(UL+UR) represents the percentage of cell death that corresponds to death by pyroptosis. (H) Pyroptosis-associated morphological characteristics were observed by scanning electron microscopy. Top scale bar, 10 μm and bottom scale bar, 5 μm. (I) Levels of IL-1β and IL-18 in cell supernatants were measured using ELISA kits. (J) The protein expression levels of NLRP3, caspase-1, GSDMD and GSDMD-N were detected by western blotting analysis. *P<0.05; **P<0.01; ***P<0.001; and ****P<0.0001. NSCLC, non-small cell lung cancer; NLRP3, NOD-like receptor pyrin domain-containing 3; GSDMD, gasdermin D; DSF, disulfram; EdU, 5-ethynyl-2'-deoxyuridine; GSDMD-N, cleaved GSDMD; CCK-8, Cell Counting Kit-8; UR, upper right; UL, upper left.

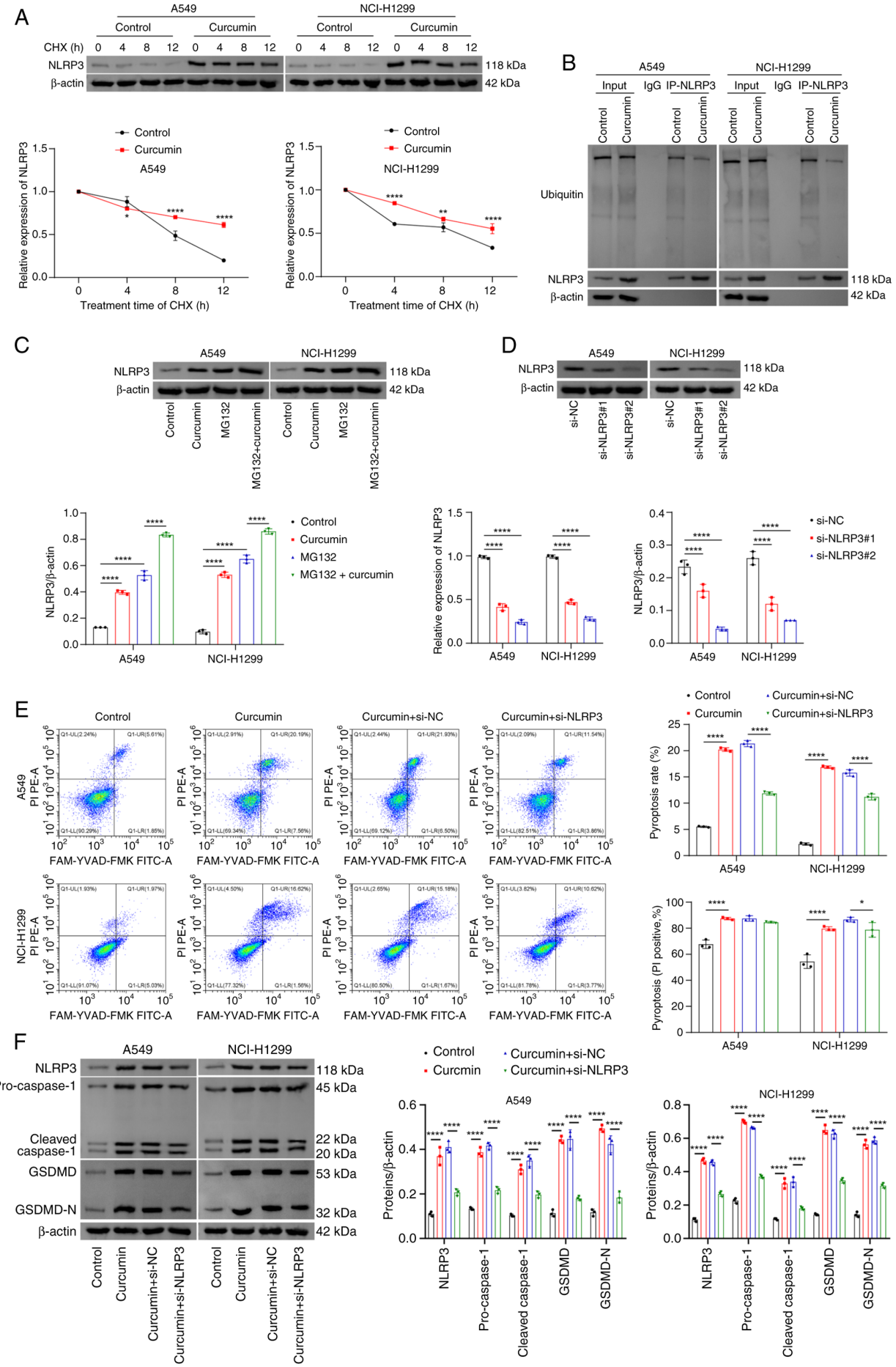

Figure 2. Continued.

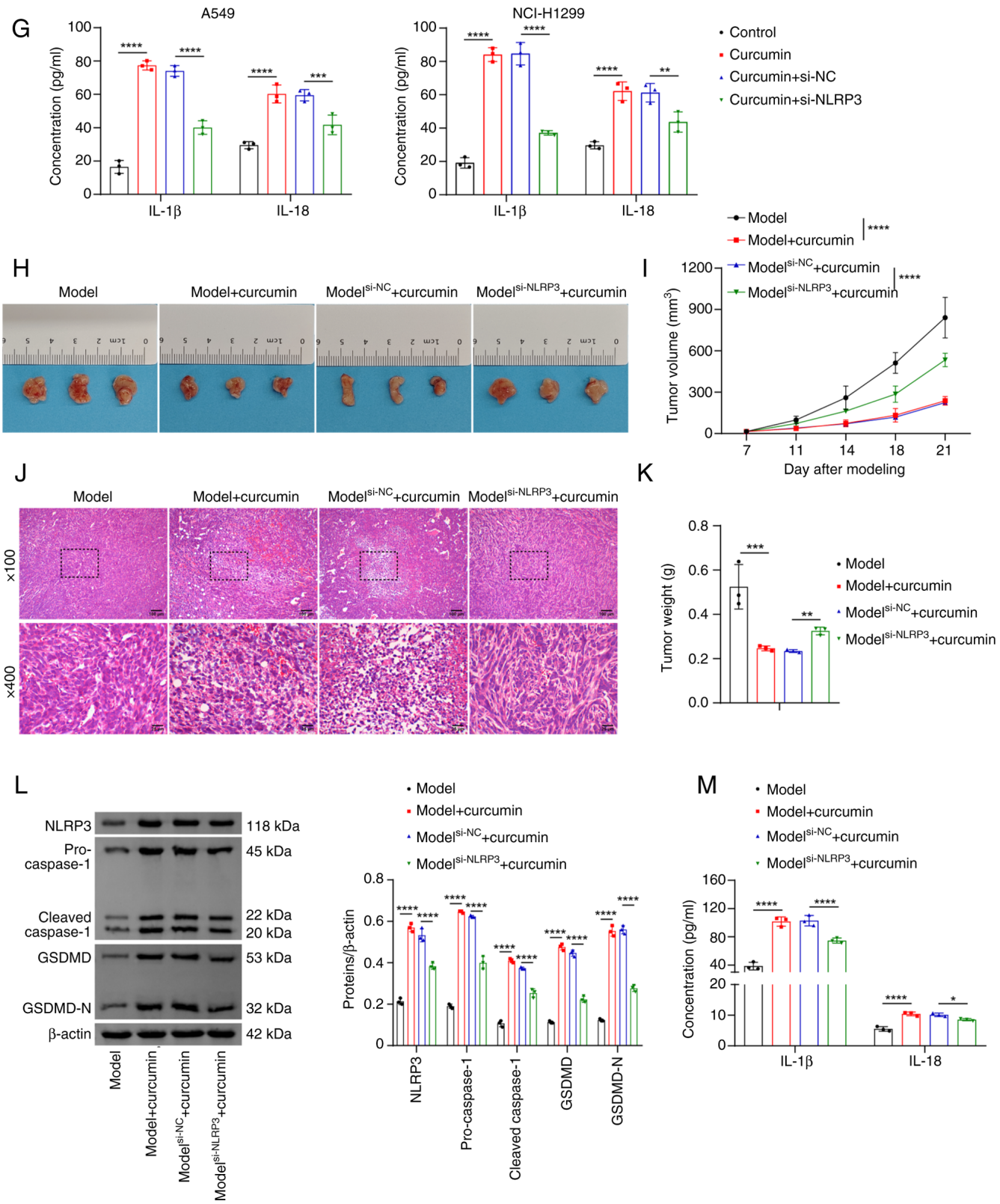

Figure 2. Curcumin induces pyroptosis in NSCLC cell lines and NSCLC nude mice cancer tissues via the upregulation of NLRP3. (A) NLRP3 protein stability was assessed by western blotting analysis. (B) The ubiquitination of NLRP3 was evaluated by Co-IP assay. (C) NLRP3 protein expression levels were measured by western blotting analysis. (D) NLRP3 knockdown efficiency was assessed by reverse transcription-quantitative PCR and western blotting analyses. (E) Pyroptosis was detected by flow cytometry, with UR/(UL+UR) representing the percentage of cell death that corresponds to death by pyroptosis. (F) The protein expression levels of NLRP3, caspase-1, GSDMD and GSDMD-N in cells were detected by western blotting analysis. (G) IL-1β and IL-18 levels in cell supernatants was measured by ELISA. (H) Representative images of the nude mice excised tumors were presented. (I) The tumor volumes were measured. (J) Pathological changes in tumor tissues were analyzed by hematoxylin and eosin staining. Top scale bar, 100 μm and bottom scale bar, 25 μm. (K) The tumor weights were measured. (L) Protein expression levels of NLRP3, caspase-1, GSDMD and GSDMD-N in tumors were detected by western blotting analysis. (M) Serum concentrations of IL-1β and IL-18 were determined using ELISA kits. *P<0.05; **P<0.01; ***P<0.001; and ****P<0.0001. NSCLC, non-small cell lung cancer; Co-IP, co-immunoprecipitation; NLRP3, NOD-like receptor pyrin domain-containing 3; GSDMD, gasdermin D; CHX, cycloheximide; si, short interfering RNA; NC, negative control; GSDMD-N, cleaved GSDMD; UR, upper right; UL, upper left.

curcumin induced pyroptosis in NSCLC cell lines and tumor tissues via upregulating NLRP3.

NLRP3 stability is regulated via Smurf2 activity. To identify additional potential targets associated with the stability and ubiquitination of NLRP3, the UbiBrowser 1.0 database was utilized, which predicted that the E3 ligase Smurf2 was involved in NLRP3 ubiquitination (Fig. 3A and B). A previous study also reported an association between Smurf2 and NSCLC (19). Consistent with the findings of the aforementioned study, the experimental results from the present study demonstrated that Smurf2 was highly expressed in NSCLC cells (Fig. 3C) and that Smurf2 could interact with NLRP3 (Fig. 3D). To further investigate the role of Smurf2 in NSCLC, Smurf2 was overexpressed or knocked down in NSCLC cells. The transfection efficiencies were confirmed, showing successful overexpression and knockdown of Smurf2, respectively (Fig. 3E). Overexpression of Smurf2 caused a significant reduction in NLRP3 protein expression levels, although this effect was significantly reversed following treatment with the proteasome inhibitor, MG132 (Fig. 3F). Additionally, Smurf2 overexpression led to an increase in the ubiquitination of NLRP3 (Fig. 3G). Compared with the si-NC group, knocking down Smurf2 led to a significantly increased expression level of NLRP3 (Fig. 3H). Moreover, the knockdown of Smurf2 markedly increased both the activation and cleavage of caspase-1 and GSDMD (Fig. 3H), significantly increasing the secretion of IL-1β and IL-18 (Fig. 3I) and cell pyroptosis (Fig. 3J) when compared with the si-NC group. However, knocking down NLRP3 markedly decreased the activation and cleavage of caspase-1 and GSDMD (Fig. 3H), the secretion of IL-1β and IL-18 (Fig. 3I), and pyroptosis (Fig. 3J) when compared with the si-Smurf2 + si-NC group. Collectively, these findings suggested that the inhibition of Smurf2 activity reduced NLRP3 ubiquitination, thereby promoting its stability and enhancing cell pyroptosis.

Curcumin targets Smurf2 to inhibit NLRP3 ubiquitination and promote pyroptosis. Building on the observed association between NLRP3 and Smurf2 in NSCLC cells, the potential interaction between curcumin and Smurf2 was subsequently further explored. The chemical structure of curcumin is shown in Fig. 4A. Molecular docking analysis confirmed that curcumin could bind to Smurf2, with a binding energy of -8.5 kcal/mol (Fig. 4B). Although the interaction between Smurf2 and NLRP3 had already been demonstrated in the present study, curcumin treatment was found to reduce the strength of this interaction (Fig. 4C). Additionally, overexpression of Smurf2 also attenuated NLRP3 expression as a consequence of their mutual interaction (Fig. 4D). Moreover, the knockdown of Smurf2 was shown to significantly enhance the ability of curcumin to stabilize NLRP3 compared with the curcumin + si-NC group, whereas overexpression of Smurf2 circumvented this effect compared with the curcumin + oe-NC group (Fig. 4E). Similarly, Smurf2 knockdown markedly augmented the curcumin-induced increase in the protein expression levels of NLRP3, caspase-1, GSDMD and GSDMD-N, as well as the secretion levels of IL-1β and IL-18 compared with the curcumin + si-NC group. On the other hand, overexpression of Smurf2 reversed these curcumin-induced effects compared with the curcumin + oe-NC group (Fig. 4F and G). Furthermore, the knockdown of Smurf2 led to a significant enhancement in the extent of pyroptosis in NSCLC cells compared with the curcumin + si-NC group, whereas Smurf2 overexpression inhibited pyroptosis compared with the curcumin + oe-NC group (Fig. 4H). Taken together, these findings suggested that curcumin both inhibited NLRP3 ubiquitination and promoted pyroptosis, in NSCLC cells through targeting Smurf2.

Curcumin inhibits NSCLC progression through regulating the Smurf2/NLRP3 axis in vivo. To validate the effects of curcumin on NSCLC progression *in vivo* and to assess the involvement of the Smurf2/NLRP3 axis, experiments were performed using NSCLC tumor-bearing modelled nude mice (Fig. 5A). These results showed that, following curcumin intervention, the tumor volumes and weights were significantly reduced. These effects were further enhanced by Smurf2 knockdown, although they were significantly reversed upon overexpressing Smurf2 (Fig. 5B). Subsequent histological analysis using H&E staining demonstrated that curcumin treatment promoted NSCLC cell death. This effect was enhanced by Smurf2 knockdown but inhibited by Smurf2 overexpression (Fig. 5C). Consistently with these findings, the expression levels of Ki67, a marker of cell proliferation (35), was markedly reduced in tumor tissues following curcumin treatment compared with the model group. Compared with the model$^{si\text{-}NC}$ + curcumin group, Smurf2 knockdown led to a further suppression of Ki67 expression, whereas Smurf2 overexpression caused a significant increase in Ki67 levels compared with the model$^{oe\text{-}NC}$ + curcumin group. Collectively, these results suggested that curcumin influenced cell proliferation in NSCLC tumors via Smurf2 regulation (Fig. 5D and E). Furthermore, Smurf2 knockdown led to a significant augmentation of the curcumin-induced increases in the protein expression levels of Smurf2, NLRP3, caspase-1, GSDMD and GSDMD-N, as well as marked increases in the secretion of IL-1β and IL-18 in tumor tissues compared with the model$^{si\text{-}NC}$ + curcumin group. On the other hand, Smurf2 overexpression reversed these curcumin-induced effects compared with the model$^{oe\text{-}NC}$ + curcumin group (Fig. 5F and G). Taken together, these findings suggested that curcumin inhibited NSCLC progression *in vivo* via regulating the Smurf2/NLRP3 axis, suggesting its potential use as a therapeutic agent for NSCLC.

Discussion

NSCLC remains one of the most prevalent cancers globally. Although mortality rates are decreasing as a result of therapeutic advances, they currently remain high (36). The present study demonstrated a potential therapeutic role of curcumin through performing a series of *in vitro* and *in vivo* experiments. These findings showed that curcumin promoted NSCLC cell pyroptosis via modulating the Smurf2/NLRP3 axis, thereby inhibiting tumor progression; moreover, these results may provide valuable insights into developing novel strategies for NSCLC therapy.

As a polyphenolic compound, curcumin has shown significant potential for cancer treatment (37). It has been reported to inhibit colorectal cancer metastasis through activating the

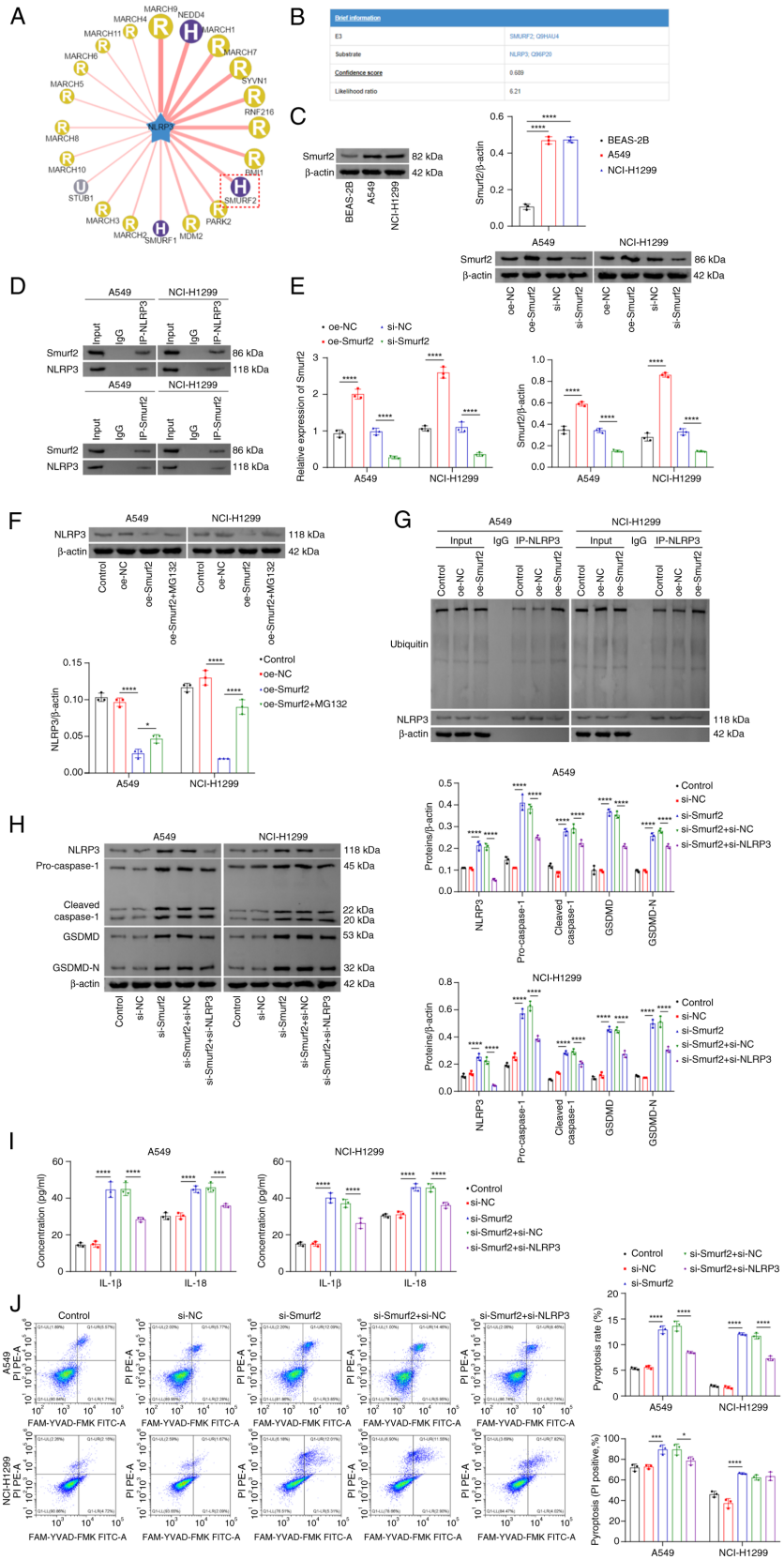

Figure 3. NLRP3 stability is regulated by Smurf2 activity. (A and B) Prediction of Smurf2 as an E3 ligase for NLRP3 was detected using the UbiBrowser 1.0 database. (C) Smurf2 protein expression levels were analyzed by western blotting. (D) Co-IP assay results confirmed the interaction between Smurf2 and NLRP3. (E) Smurf2 transfection efficiency was determined via both reverse transcription-quantitative PCR and western blotting analyses. (F) The detection of NLRP3 protein expression levels was performed using western blotting analysis. (G) The ubiquitination of NLRP3 was detected by Co-IP assay. (H) The protein expression levels of NLRP3, caspase-1, GSDMD and GSDMD-N in cells were determined using western blotting analysis. (I) Secreted IL-1β and IL-18 levels were measured using ELISA kits. (J) Flow cytometric analysis was performed for the detection of cell pyroptosis. The UR/(UL+UR) represents the percentage of cell death that corresponds to death by pyroptosis. *P<0.05; ***P<0.001; and ****P<0.0001. NLRP3, NOD-like receptor pyrin domain-containing 3; Smurf2, Smad ubiquitination regulatory factor 2; Co-IP, co-immunoprecipitation; GSDMD, gasdermin D; oe, overexpression; NC, negative control; si, short interfering RNA; GSDMD-N, cleaved GSDMD; UR, upper right; UL, upper left.

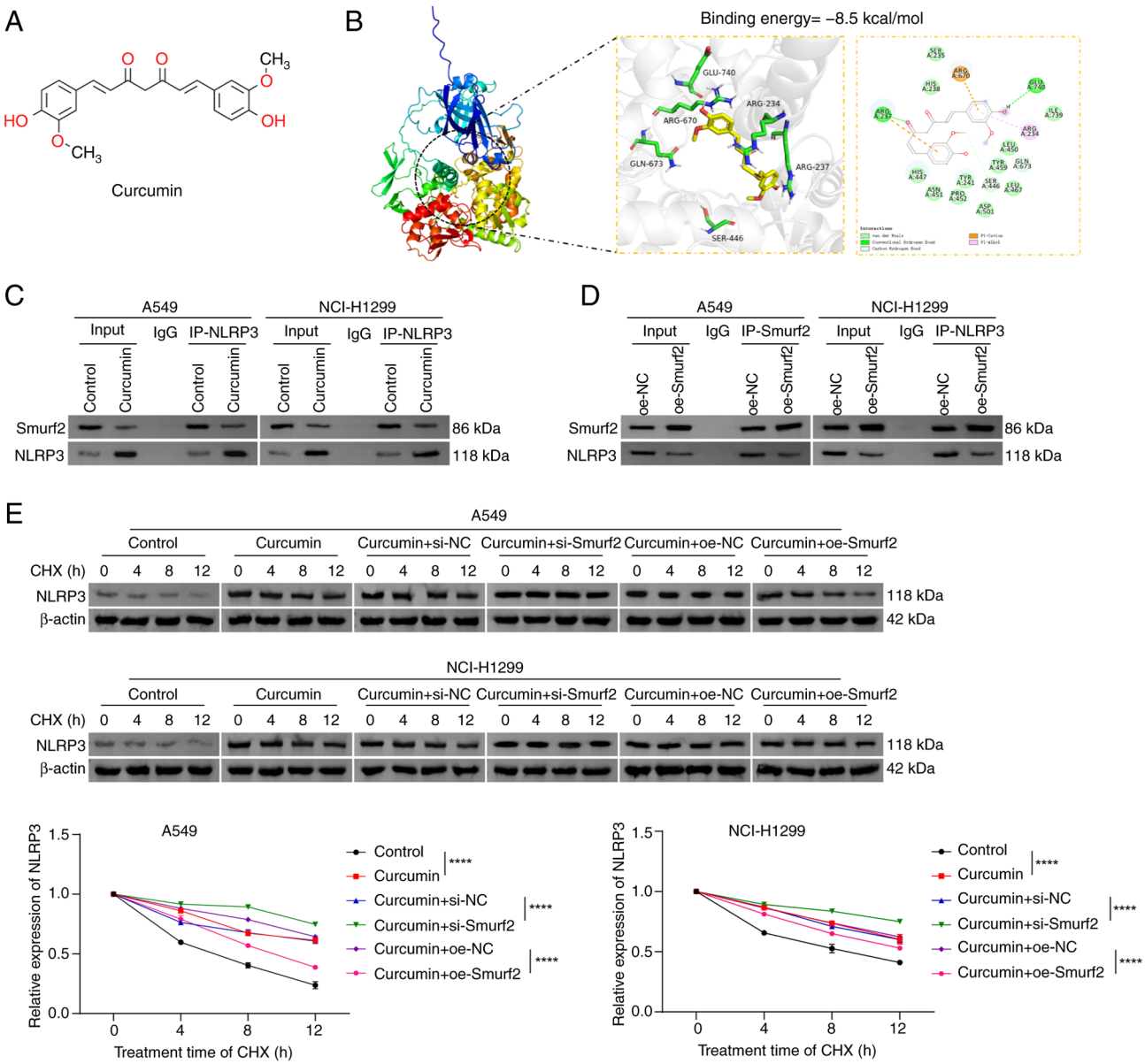

Figure 4. Continued.

reactive oxygen species/Kelch-like ECH-associated protein 1/nuclear factor erythroid 2-related factor 2/microRNA (miR)-34a/b/c pathway (38). In esophageal squamous cell carcinoma, curcumin has been shown to alleviate cancer progression by downregulating the circular RNA nuclear receptor interacting protein 1/miR-532-3p/AKT signaling pathway (39). In head and neck squamous cell carcinoma, curcumin exerts anticancer effects through modulating the tumor microenvironment (39). Similarly, the present study showed that curcumin inhibited NSCLC cell growth via promoting pyroptosis and the addition of inhibitors targeting pyroptosis-associated factors led to a reversal of curcumin's effects, thereby highlighting its mechanistic role in inducing apoptosis and pyroptosis in NSCLC cells.

NLRP3 is an important component of the inflammasome protein complex, which promotes the maturation and secretion of pro-IL-1β and pro-IL-18, the precursor forms of IL-1β and IL-18 (40). As an essential regulator of pyroptosis (41), NLRP3 has been shown to mediate pyroptosis through natural active substances in a variety of cancer types. For example, anthocyanin was shown to activate pyroptosis in oral squamous cell carcinoma cells via NLRP3, caspase-1 and GSDMD signaling (42). Similarly, polyphyllin VI was found to induce caspase-1-mediated pyroptosis in NSCLC through inducing the NLRP3/GSDMD axis (43) and citric acid triggers pyroptosis in ovarian cancer (OC) cells via caspase-4, NLRP3 and GSDMD signaling (44). In the present study, curcumin increased the stability of NLRP3 and reduced its level of ubiquitination, underscoring its regulatory role in pyroptosis. Both *in vitro* and *in vivo* experiments demonstrated that knockdown of NLRP3 reversed the effects of curcumin-induced pyroptosis, including the activation and cleavage of caspase-1 and GSDMD, increased secretion of IL-1β and IL-18 and suppression of NSCLC tumor growth in nude mice. Collectively, these results underlined the pivotal role of NLRP3 in curcumin-mediated pyroptosis, suggesting

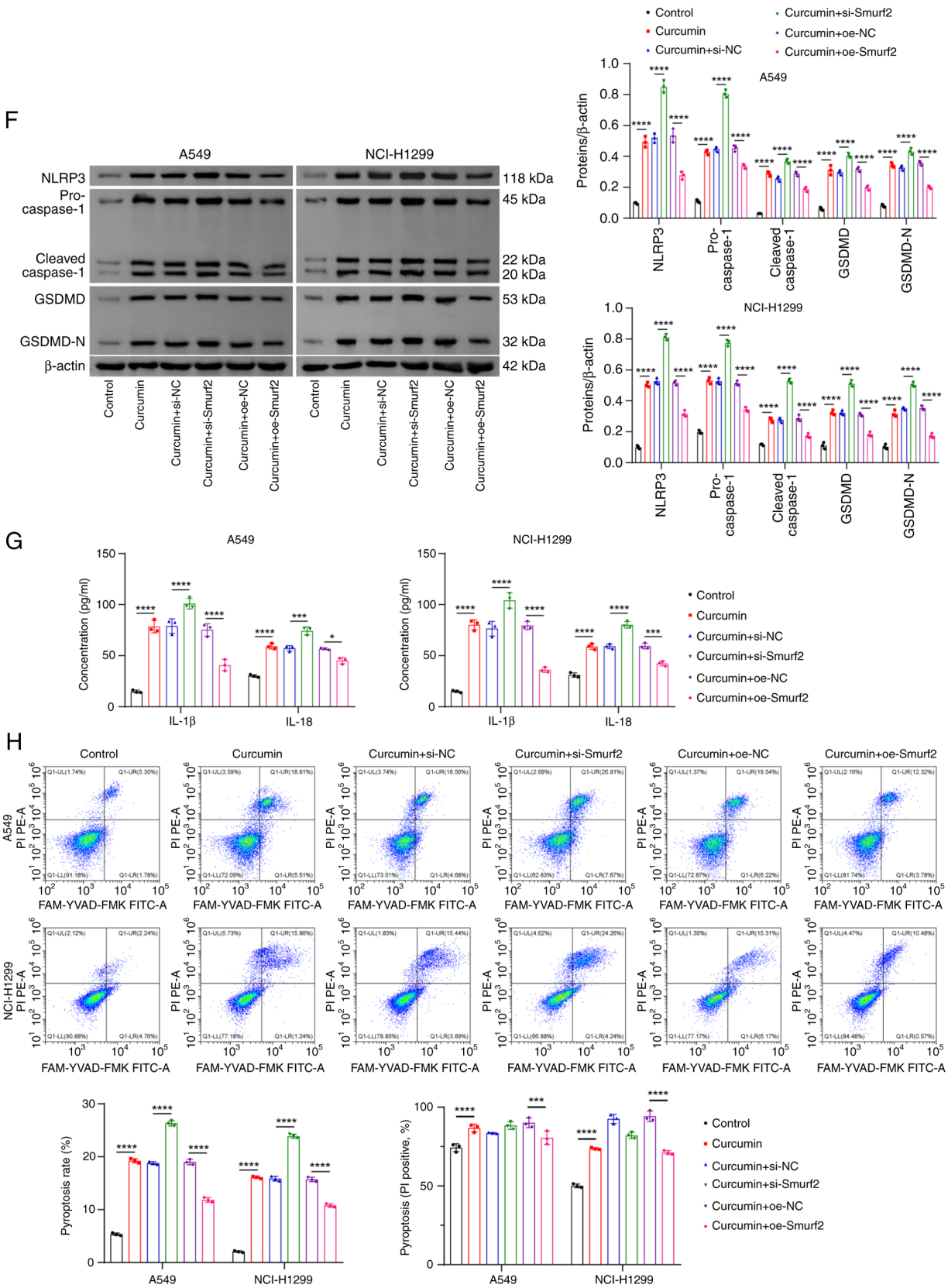

Figure 4. Curcumin targets Smurf2 to inhibit NLRP3 ubiquitination and promote pyroptosis. (A) The chemical structure of curcumin. (B) Molecular docking analysis was performed, showing the binding of curcumin to Smurf2. (C and D) Co-IP analysis was performed for the interaction strength between Smurf2 and NLRP3. (C) The immunoprecipitation protein was NLRP3. (D) The immunoprecipitation protein was Smurf2. (E) The protein expression levels of NLRP3 were assessed using western blot analysis. CHX was used to detect the protein stabilities of NLRP3. (F) The protein expression levels of NLRP3, caspase-1, GSDMD and GSDMD-N were determined using western blot analysis. (G) The ability of cells to secrete IL-1β and IL-18 was measured using ELISA kits. (H) Cell pyroptosis was determined using flow cytometric analysis. UR/(UL+UR) represents the percentage of cell death that corresponds to death by pyroptosis. *P<0.05; ***P<0.001; and ****P<0.0001. Smurf2, Smad ubiquitination regulatory factor 2; NLRP3, NOD-like receptor pyrin domain-containing 3; Co-IP, co-immunoprecipitation; IP, immunoprecipitated; GSDMD, gasdermin D; si, short interfering RNA; NC, negative control; oe, overexpression; GSDMD-N, cleaved GSDMD; CHX, cycloheximide; UR, upper right; UL, upper left.

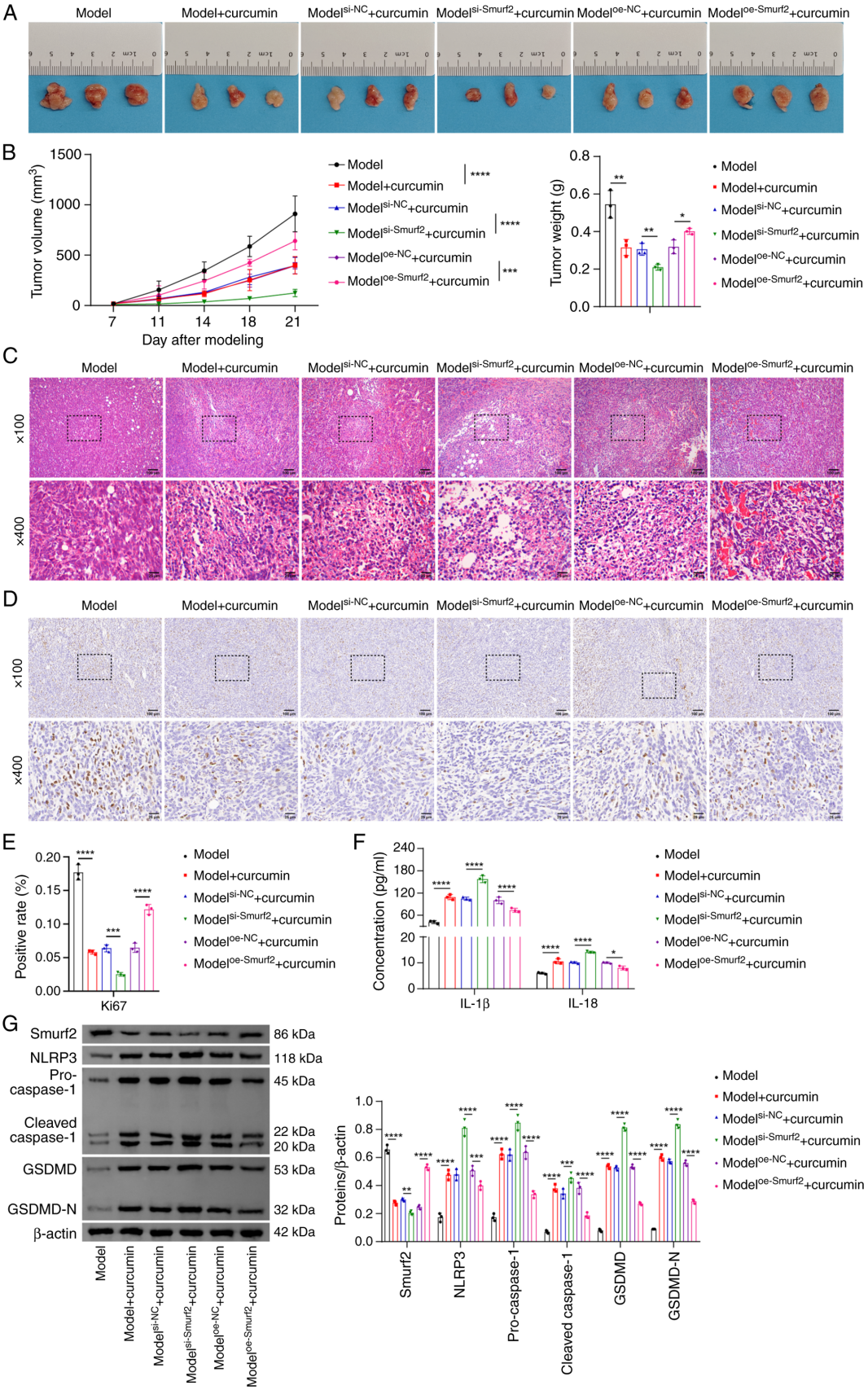

Figure 5. Curcumin inhibits non-small cell lung cancer progression by regulating the Smurf2/NLRP3 axis *in vivo*. (A) Representative images of tumors are shown. (B) Tumor volume and weight measurements are shown. (C) Pathological examination of tumor tissues was performed by hematoxylin and eosin staining. Top scale bar, 100 μm and bottom scale bar, 25 μm. (D and E) Ki67 expression in tumors was assessed using immunohistochemical analysis. Top scale bar, 100 μmand bottom scale bar, 25 μm. (F) Serum concentrations of IL-1β and IL-18 were measured using ELISA kits. (G) The protein expression levels of Smurf2, NLRP3, caspase-1, GSDMD and GSDMD in tumors were detected by western blotting analysis. *P<0.05; **P<0.01; ***P<0.001; and ****P<0.0001. Smurf2, Smad ubiquitination regulatory factor 2; NLRP3, NOD-like receptor pyrin domain-containing 3; GSDMD, gasdermin D; GSDMD-N, cleaved GSDMD; oe, overexpression; NC, negative control; si, short interfering RNA.

that targeting NLRP3 may be a promising strategy for NSCLC treatment.

Upon western blot analysis, cleaved-caspase-1 appears with two bands. This is due to the fact that pro-caspase-1 undergoes cleavage upon activation, generating several fragments of different sizes, including fragments of 20 and 22 kDa in size (45). These fragments represent the cleavage products of caspase-1 and they result in the formation of the active caspase-1 enzyme (45). Furthermore, changes in the expression level of pro-caspase-1 reflect the activation status of caspase-1. The expression level of cleaved-caspase-1 has been shown to reflect the activity level of caspase-1 more directly during apoptosis and the inflammatory response (46). The independent detection of the expression levels of pro-caspase-1 and cleaved-caspase-1 in the present study has contributed to a more detailed understanding of the underlying regulatory mechanisms of the caspase-1 signaling pathway by showing the effects of certain factors, such as curcumin and Smurf2, on the cleavage and activation of caspase-1. Therefore, the results for pro-caspase-1 and cleaved-caspase-1, the 20 and 22 kDa cleaved products, respectively, were presented individually.

The investigation of NLRP3 ubiquitination and deubiquitination has emerged as an important area of research in the context of inflammatory diseases (15). The UbiBrowser 1.0 database was utilized to identify potential E3 ligases that interacted with NLRP3, which predicted that Smurf2 was among the candidate E3 ligases. Smurf2 is a ubiquitin E3 ligase involved in the degradation of various proteins via the 26S proteasome (47). Moreover, other studies have demonstrated diverse roles for Smurf2 in cancer. Xie *et al* (45) reported that Smurf2 mediates glutathione S-transferase P1 ubiquitination, leading to ferroptosis in cancer cells through a glutathione peroxidase 4-independent mechanism. Han *et al* (48) showed that Smurf2 interacts with DNA-binding inhibitor 2 (ID2) in lung cancer cells, thereby promoting the polyubiquitination and degradation of ID2 via the ubiquitin-proteasome pathway, which ultimately induces cell cycle arrest. Furthermore, Pi *et al* (49) found that the deletion of Smurf2 expression in human OC reduces the ubiquitination of receptor for activated C kinase 1, thereby promoting OC progression. In the present study, it was demonstrated that Smurf2 interacted with NLRP3 and that the upregulation of Smurf2 enhanced NLRP3 ubiquitination. Furthermore, Smurf2 knockdown promoted NLRP3 expression and cell pyroptosis, demonstrating that Smurf2 can both regulate NLRP3 ubiquitination and exert a significant impact on the process of pyroptosis in NSCLC cells.

A previous study showed that curcumin can inhibit TGF-β/Smad signaling through activating autophagy (50). Additionally, Smad2 and Smad3 degradation may occur through Smurf2-mediated ubiquitination and proteasomal degradation (50). The associated involvement of curcumin and Smurf2 was also demonstrated in a rat model of paraquat-induced pulmonary fibrosis, where curcumin was found to modulate Smurf2 activity (51). In the present study, molecular docking analysis demonstrated that curcumin binds to Smurf2. Additionally, treatment with curcumin inhibited the strength of the interaction between Smurf2 and NLRP3. Knockdown of Smurf2 led to an augmentation of curcumin's effects on the stability of NLRP3, pyroptosis and the expression of pyroptosis-associated factors in NSCLC cells. On the other hand, the overexpression of Smurf2 led to a reversal of these effects, underscoring the crucial role of Smurf2 in curcumin-mediated regulation of NLRP3-dependent pyroptosis. Based on the *in vivo* mouse model experiments, curcumin treatment reduced both the volume and the weight of NSCLC tumors, decreased the level of Ki67 expression and increased the expression levels of NLRP3 and pyroptosis-associated factors. These findings were consistent with the results obtained from the *in vitro* experiments, further supporting the potential of curcumin as a therapeutic agent for NSCLC. Moreover, the *in vivo* experiments confirmed that curcumin inhibited NSCLC progression by modulating the Smurf2/NLRP3 axis, thereby offering a novel perspective for NSCLC treatment.

However, the present study had certain limitations. First, the precise mechanism underlying Smurf2's interactions with other proteins requires further, more detailed studies, such as the GSDMD protein. Secondly, clinical studies are required to confirm the efficacy of curcumin in treating NSCLC. These challenges highlight areas for future research and should be the focus for ongoing efforts aiming to address these gaps in current knowledge.

In conclusion, the present study showed that curcumin promoted NLRP3-dependent pyroptosis in NSCLC cells through inhibiting Smurf2 activity, highlighting a potential mechanism underlying the antitumor effects exerted by curcumin and suggesting novel therapeutic targets and strategies for the treatment of NSCLC.

Acknowledgements

Not applicable.

Funding

This work was supported by the Key Research Project of Nanhua University Funding (grant no. nk2020108).

Availability of data and materials

The data generated in the present study may be requested from the corresponding author.

Authors' contributions

YX, SZ, XT and XD performed the experiments and collected data. YX analyzed the data and wrote the manuscript. XD revised the manuscript. All authors read and approved the final version of the manuscript. YX and XD confirm the authenticity of all the raw data.

Ethics approval and consent to participate

Experiments in the present study were approved by the Medical Ethics Committee of the Second Affiliated Hospital, University of South China (approval no. NHFE2022010601; Hengyang, China).

Patient consent for publication

Not applicable.

Competing interests

The authors declare that they have no competing interests.

References

1. Srivastava S, Mohanty A, Nam A, Singhal S and Salgia R: Chemokines and NSCLC: Emerging role in prognosis, heterogeneity, and therapeutics. Semin Cancer Biol 86: 233-246, 2022.
2. Ganti AK, Klein AB, Cotarla I, Seal B and Chou E: Update of incidence, prevalence, survival, and initial treatment in patients with non-small cell lung cancer in the US. JAMA Oncol 7: 1824-1832, 2021.
3. Clark SB and Alsubait S: Non-small cell lung cancer. In: StatPearls. StatPearls Publishing LLC., Treasure Island, FL, 2024.
4. Jonna S and Subramaniam DS: Molecular diagnostics and targeted therapies in non-small cell lung cancer (NSCLC): An update. Discov Med 27: 167-170, 2019.
5. Huang X, Wang Y, Yang W, Dong J and Li L: Regulation of dietary polyphenols on cancer cell pyroptosis and the tumor immune microenvironment. Front Nutr 9: 974896, 2022.
6. Kotha RR and Luthria DL: Curcumin: Biological, pharmaceutical, nutraceutical, and analytical aspects. Molecules 24: 2930, 2019.
7. Wan Mohd Tajuddin WNB, Lajis NH, Abas F, Othman I and Naidu R: Mechanistic understanding of curcumin's therapeutic effects in lung cancer. Nutrients 11: 2989, 2019.
8. Fang Y, Tian S, Pan Y, Li W, Wang Q, Tang Y, Yu T, Wu X, Shi Y, Ma P and Shu Y: Pyroptosis: A new frontier in cancer. Biomed Pharmacother 121: 109595, 2020.
9. Rao Z, Zhu Y, Yang P, Chen Z, Xia Y, Qiao C, Liu W, Deng H, Li J, Ning P and Wang Z: Pyroptosis in inflammatory diseases and cancer. Theranostics 12: 4310-4329, 2022.
10. Guo J, Yan W, Duan H, Wang D, Zhou Y, Feng D, Zheng Y, Zhou S, Liu G and Qin X: Therapeutic effects of natural products on liver cancer and their potential mechanisms. Nutrients 16: 1642, 2024.
11. Yuan R, Zhao W, Wang QQ, He J, Han S, Gao H, Feng Y and Yang S: Cucurbitacin B inhibits non-small cell lung cancer in vivo and in vitro by triggering TLR4/NLRP3/GSDMD-dependent pyroptosis. Pharmacol Res 170: 105748, 2021.
12. Duan H, Jiang L, Sun X, Liu X, Yang G, Sun X, Cheng T, Ji Y, Zhang F, Du Y, *et al*: Curcumin induces MCF-7 cells pyroptosis via autophagy/CTSB/NLRP3/caspase-1/GSDMD signaling pathway in vitro and vivo. J Vet Heal Sci 3: 250-261, 2022.
13. Feng SH, Zhao B, Zhan X, Li RH, Yang Q, Wang SM and Li A: Quercetin-induced pyroptosis in colon cancer through NEK7-mediated NLRP3 inflammasome-GSDMD signaling pathway activation. Am J Cancer Res 14: 934-958, 2024.
14. Krishnan SM, Ling YH, Huuskes BM, Ferens DM, Saini N, Chan CT, Diep H, Kett MM, Samuel CS, Kemp-Harper BK, *et al*: Pharmacological inhibition of the NLRP3 inflammasome reduces blood pressure, renal damage, and dysfunction in salt-sensitive hypertension. Cardiovasc Res 115: 776-787, 2019.
15. Akther M, Haque ME, Park J, Kang TB and Lee KH: NLRP3 ubiquitination-A new approach to target NLRP3 inflammasome activation. Int J Mol Sci 22: 8780, 2021.
16. Liu X, Fang Y, Lv X, Hu C, Chen G, Zhang L, Jin B, Huang L, Luo W, Liang G and Wang Y: Deubiquitinase OTUD6A in macrophages promotes intestinal inflammation and colitis via deubiquitination of NLRP3. Cell Death Differ 30: 1457-1471, 2023.
17. Xu T, Yu W, Fang H, Wang Z, Chi Z, Guo X, Jiang D, Zhang K, Chen S, Li M, *et al*: Ubiquitination of NLRP3 by gp78/Insig-1 restrains NLRP3 inflammasome activation. Cell Death Differ 29: 1582-1595, 2022.
18. Yan B, Jin Y, Mao S, Zhang Y, Yang D, Du M and Yin Y: Smurf2-mediated ubiquitination of FOXO4 regulates oxygen-glucose deprivation/reperfusion-induced pyroptosis of cortical neurons. Curr Neurovasc Res 20: 443-452, 2023.
19. Chaudhary KR, Kinslow CJ, Cheng H, Silva JM, Yu J, Wang TJ, Hei TK, Halmos B and Cheng SK: Smurf2 inhibition enhances chemotherapy and radiation sensitivity in non-small-cell lung cancer. Sci Rep 12: 10140, 2022.
20. Yang FR, Li SY, Hu XW, Li XR and Li HJ: Identifying the antitumor effects of curcumin on lung adenocarcinoma using comprehensive bioinformatics analysis. Drug Des Devel Ther 16: 2365-2382, 2022.
21. Schamberger B and Plaetzer K: Photofungizides based on curcumin and derivates thereof against *candida albicans* and *aspergillus niger*. Antibiotics (Basel) 10: 1315, 2021.
22. Galvao J, Davis B, Tilley M, Normando E, Duchen MR and Cordeiro MF: Unexpected low-dose toxicity of the universal solvent DMSO. FASEB J 28: 1317-1330, 2014.
23. Li M, Wu R, Wang L, Zhu D, Liu S, Wang R, Deng C, Zhang S, Chen M, Lu R, *et al*: Usenamine A triggers NLRP3/caspase-1/GSDMD-mediated pyroptosis in lung adenocarcinoma by targeting the DDX3X/SQSTM1 axis. Aging (Albany NY) 16: 1663-1684, 2024.
24. Leng B, Zhang Y, Liu X, Zhang Z, Liu Y, Wang H and Lu M: Astragaloside IV suppresses high glucose-induced NLRP3 inflammasome activation by inhibiting TLR4/NF-κB and CaSR. Mediators Inflamm 2019: 1082497, 2019.
25. Zhao C, Liang F, Ye M, Wu S, Qin Y, Zhao L, Zhang L, He J, Cen L and Lin F: GSDMD promotes neutrophil extracellular traps via mtDNA-cGAS-STING pathway during lung ischemia/reperfusion. Cell Death Discov 9: 368, 2023.
26. Ge X, Cai F, Shang Y, Chi F, Xiao H, Xu J, Fu Y and Bai C: PARK2 attenuates house dust mite-induced inflammatory reaction, pyroptosis and barrier dysfunction in BEAS-2B cells by ubiquitinating NLRP3. Am J Transl Res 13: 326-335, 2021.
27. Zhang X, Zhang K and Zhang Y: Pigment epithelium-derived factor facilitates NLRP3 inflammasome activation through downregulating cytidine monophosphate kinase 2: A potential treatment strategy for missed abortion. Int J Mol Med 45: 1436-1446, 2020.
28. Chen Z, Li P, Shen L and Jiang X: Heat shock protein B7 (HSPB7) inhibits lung adenocarcinoma progression by inhibiting glycolysis. Oncol Rep 50: 196, 2023.
29. Shih KC, Chan HW, Wu CY and Chuang HY: Curcumin enhances the abscopal effect in mice with colorectal cancer by acting as an immunomodulator. Pharmaceutics 15: 1519, 2023.
30. Kollias NS, Hess WJ, Johnson CL, Murphy M and Golab G: A literature review on current practices, knowledge, and viewpoints on pentobarbital euthanasia performed by veterinarians and animal remains disposal in the United States. J Am Vet Med Assoc 261: 733-738, 2023.
31. Cai B, Zhao J, Zhang Y, Liu Y, Ma C, Yi F, Zheng Y, Zhang L, Chen T, Liu H, *et al*: USP5 attenuates NLRP3 inflammasome activation by promoting autophagic degradation of NLRP3. Autophagy 18: 990-1004, 2022.
32. Schmittgen TD and Livak KJ: Analyzing real-time PCR data by the comparative C(T) method. Nat Protoc 3: 1101-1108, 2008.
33. Calibasi-Kocal G, Pakdemirli A, Bayrak S, Ozupek NM, Sever T, Basbinar Y, Ellidokuz H and Yigitbasi T: Curcumin effects on cell proliferation, angiogenesis and metastasis in colorectal cancer. J BUON 24: 1482-1487, 2019.
34. Jing X, Yun Y, Ji X, Yang E and Li P: Pyroptosis and inflammasome-related genes-*NLRP3*, *NLRC4* and *NLRP7* polymorphisms were associated with risk of lung cancer. Pharmgenomics Pers Med 16: 795-804, 2023.
35. Menon SS, Guruvayoorappan C, Sakthivel KM and Rasmi RR: Ki-67 protein as a tumour proliferation marker. Clin Chim Acta 491: 39-45, 2019.
36. Howlader N, Forjaz G, Mooradian MJ, Meza R, Kong CY, Cronin KA, Mariotto AB, Lowy DR and Feuer EJ: The effect of advances in lung-cancer treatment on population mortality. N Engl J Med 383: 640-649, 2020.
37. Giordano A and Tommonaro G: Curcumin and cancer. Nutrients 11: 2376, 2019.
38. Liu C, Rokavec M, Huang Z and Hermeking H: Curcumin activates a ROS/KEAP1/NRF2/miR-34a/b/c cascade to suppress colorectal cancer metastasis. Cell Death Differ 30: 1771-1785, 2023.
39. Luo T, Guan H, Liu J, Wang J and Zhang Y: Curcumin inhibits esophageal squamous cell carcinoma progression through down-regulating the circNRIP1/miR-532-3p/AKT pathway. Environ Toxicol 38: 2705-2716, 2023.
40. Fu J and Wu H: Structural Mechanisms of NLRP3 inflammasome assembly and activation. Annu Rev Immunol 41: 301-316, 2023.
41. Zheng X, Wan J and Tan G: The mechanisms of NLRP3 inflammasome/pyroptosis activation and their role in diabetic retinopathy. Front Immunol 14: 1151185, 2023.

42. Yue E, Tuguzbaeva G, Chen X, Qin Y, Li A, Sun X, Dong C, Liu Y, Yu Y, Zahra SM, *et al*: Anthocyanin is involved in the activation of pyroptosis in oral squamous cell carcinoma. Phytomedicine 56: 286-294, 2019.
43. Teng JF, Mei QB, Zhou XG, Tang Y, Xiong R, Qiu WQ, Pan R, Law BY, Wong VK, Yu CL, *et al*: Polyphyllin VI induces caspase-1-mediated pyroptosis via the induction of ROS/NF-κB/NLRP3/GSDMD signal axis in non-small cell lung cancer. Cancers (Basel) 12: 193, 2020.
44. Wang X, Yin Y, Qian W, Peng C, Shen S, Wang T and Zhao S: Citric acid of ovarian cancer metabolite induces pyroptosis via the caspase-4/TXNIP-NLRP3-GSDMD pathway in ovarian cancer. FASEB J 36: e22362, 2022.
45. Xie W, Peng M, Liu Y, Zhang B, Yi L and Long Y: Simvastatin induces pyroptosis via ROS/caspase-1/GSDMD pathway in colon cancer. Cell Commun Signal 21: 329, 2023.
46. Liu X, Li M, Chen Z, Yu Y, Shi H, Yu Y, Wang Y, Chen R and Ge J: Mitochondrial calpain-1 activates NLRP3 inflammasome by cleaving ATP5A1 and inducing mitochondrial ROS in CVB3-induced myocarditis. Basic Res Cardiol 117: 40, 2022.
47. Chae DK, Park J, Cho M, Ban E, Jang M, Yoo YS, Kim EE, Baik JH and Song EJ: MiR-195 and miR-497 suppress tumorigenesis in lung cancer by inhibiting SMURF2-induced TGF-β receptor I ubiquitination. Mol Oncol 13: 2663-2678, 2019.
48. Han M, Guo Y, Li Y, Zeng Q, Zhu W and Jiang J: SMURF2 facilitates ubiquitin-mediated degradation of ID2 to attenuate lung cancer cell proliferation. Int J Biol Sci 19: 3324-3340, 2023.
49. Pi Y, Feng Q, Sun F, Wang Z, Zhao Y, Chen D, Liu Y and Lou G: Loss of SMURF2 expression enhances RACK1 stability and promotes ovarian cancer progression. Cell Death Differ 30: 2382-2392, 2023.
50. Kong D, Zhang Z, Chen L, Huang W, Zhang F, Wang L, Wang Y, Cao P and Zheng S: Curcumin blunts epithelial-mesenchymal transition of hepatocytes to alleviate hepatic fibrosis through regulating oxidative stress and autophagy. Redox Biol 36: 101600, 2020.
51. Chen H, Yang R, Tang Y and Fu X: Effects of curcumin on artery blood gas index of rats with pulmonary fibrosis caused by paraquat poisoning and the expression of Smad 4, Smurf 2, interleukin-4 and interferon-γ. Exp Ther Med 17: 3664-3670, 2019.